




Article

Ray Tracing of the New Multi-Modal X-ray Imaging Beamline PolyX at SOLARIS National Synchrotron Radiation Centre

Filip Kosiorowski ^{1,2} , Paweł Wróbel ^{1,2,*} , Tomasz Kołodziej ¹, Katarzyna M. Sowa ¹,
Magdalena Szczerbowska-Boruchowska ² and Paweł Korecki ^{1,3} 

¹ SOLARIS National Synchrotron Radiation Centre, ul. Czerwone Maki 98, 30-392 Kraków, Poland; k.sowa@uj.edu.pl (K.M.S.); pawel.korecki@uj.edu.pl (P.K.)

² Faculty of Physics and Applied Computer Science, AGH University of Science and Technology, al. Mickiewicza 30, 30-059 Kraków, Poland

³ Institute of Physics, Jagiellonian University, ul. Łojasiewicza 11, 30-348 Kraków, Poland

* Correspondence: pwrobel@agh.edu.pl

Abstract: The aim of the presented research is to evaluate the potential performance of a new bending magnet X-ray beamline—PolyX, designed for microimaging and microspectroscopy at the National Synchrotron Radiation Centre SOLARIS in Krakow. Due to the short beamline length (<15 m), PolyX uses compact polycapillary and single-bounce monocapillary optics for X-ray focusing in the 4–15 keV energy range. Polycapillary optics require a dedicated approach for an efficient simulation of X-ray propagation in multiple capillary channels. Therefore, the PolyX beamline was ray traced by combining XRT (XRayTracer) and polycap libraries. In addition, to estimate the X-ray fluorescence spectra excited by focused beams, Monte Carlo simulations were conducted using XMI-MSIM. All simulations were aimed to estimate the crucial X-ray beam properties, i.e., the flux, the spot size, and the energy spectrum, for monochromatic and polychromatic X-ray beams.

Keywords: synchrotron beamline; ray-tracing simulations; Monte-Carlo simulations



Citation: Kosiorowski, F.; Wróbel, P.; Kołodziej, T.; Sowa, K.M.; Szczerbowska-Boruchowska, M.; Korecki, P. Ray Tracing of the New Multi-Modal X-ray Imaging Beamline PolyX at SOLARIS National Synchrotron Radiation Centre. *Appl. Sci.* **2024**, *14*, 7486. <https://doi.org/10.3390/app14177486>

Academic Editor: Alexander N. Pisarchik

Received: 23 July 2024

Revised: 19 August 2024

Accepted: 21 August 2024

Published: 24 August 2024



Copyright: © 2024 by the authors. Licensee MDPI, Basel, Switzerland. This article is an open access article distributed under the terms and conditions of the Creative Commons Attribution (CC BY) license (<https://creativecommons.org/licenses/by/4.0/>).

1. Introduction

SOLARIS is a synchrotron radiation facility with a 1.5 GeV storage ring located in Krakow, southern Poland. It was commissioned in 2015, and it is a third-generation source of soft X-rays with a critical photon energy of 2 keV. Currently, there are five active beamlines and three under construction/commissioned [1]. One of them is PolyX [2]—a simple and compact beamline that aims to provide both unfocused and focused beams from the bending magnet for X-ray microimaging and X-ray microspectroscopy experiments. The main techniques available with PolyX are μ -XRF, μ -XAS, μ -CT with absorption and phase contrast as well as plenoptic X-ray imaging [3]. The beam focusing is achieved using polycapillary optics. Those very compact devices use the effect of total external reflection of X-rays inside thousands of small bent hollow glass tubes. PolyX will take advantage of the very high acceptance of polycapillary lenses, allowing for it to achieve highly intense white, pink, or monochromatic 4–15 keV X-rays focused down to 10 μ m. For better focusing (down to 2 μ m), an ellipsoidal single-bounce monocapillary lens will be used.

In the field of X-ray physics, ray tracing refers to the simulation of X-ray beams propagating through different materials and optical components. Ray-tracing simulations have become an essential tool in X-ray physics for designing and optimizing synchrotron beamlines [4–7] and optical elements, including single-bounce capillary devices [8–10] as well as polycapillary optics [11–13]. Ray-tracing simulations allow for the evaluation of X-ray beam properties such as flux, spot size, and energy spectrum, which are crucial for optimizing the performance of a beamline. Moreover, by simulating the entire beamline, it is possible to identify and correct potential issues before the actual installation of the beamline, as well as to predict the performance of the beamline.

The goal of this research is to use ray tracing to predict the performance of the PolyX beamline, specifically the photon flux on the sample (in both polychromatic and monochromatic modes) and the achievable beam size with different available polycapillary lenses, as well as single-bounce ellipsoidal monocapillary. Furthermore, the ray-tracing model will enable the simulation of the beam characteristics in all possible configurations of the adjustable beamline components, such as filters and slits.

In this paper, for PolyX beamline ray tracing, we used the XRT toolkit [5]. XRT is a Python-based software library for beamline simulation and analysis in X-ray regimes. It provides the classes for many beamline elements, the propagation engine in ray and wave approximations with full account for shapes and material properties, and high-quality visualization capabilities. While XRT enables the user to simulate X-ray propagation inside polycapillary optics, such calculations are very time-consuming. Therefore, we used XRT (for simulation of standard beamline components) in conjunction with the polycap library [7]. Polycap is a multithreaded Monte Carlo-based X-ray ray tracing code dedicated to the simulation of polycapillary optics. Moreover, to evaluate the performance of the beamline in fast, high-resolution μ -XRF mapping, additional simulations of X-ray spectra with the XMI-MSIM [14] tool were performed.

2. Beamline Description

The source of the PolyX beamline is a 1.31 T bending magnet from the SOLARIS storage ring. The detailed information about the source is given in Table 1 and the scheme of the beamline is provided in Figure 1. The beamline optics are designed to deliver either a polychromatic white beam or a monochromatized beam to the end station. Two types of interchangeable monochromators are planned: a double crystal monochromator (DCM) and a double multilayer monochromator (DMM). The list of all main components of the beamline with corresponding distances from the bending magnet is shown in Table 2.

Table 1. Bending magnet (X-ray source) parameters used in simulations.

Parameter	Value
Electron beam energy	1.5 GeV
Maximum current	500 mA
Electron beam sizes (σ_x , σ_z)	44 μm , 30 μm
Electron beam emittance (ϵ_x , ϵ_z)	8.05 nm \cdot rad, 0.065 nm \cdot rad
BM magnetic field	1.31 T

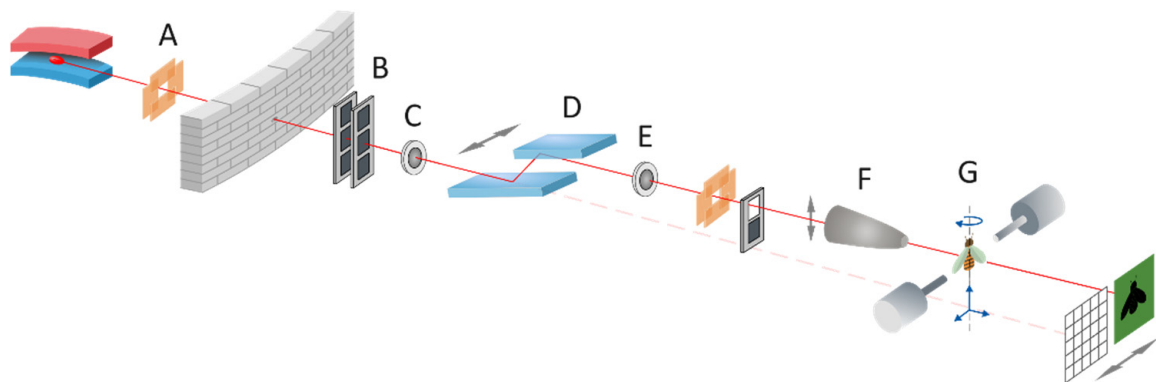


Figure 1. The scheme of PolyX beamline. A—white beam slits, B—white beam filters, C—beam window 1, D—monochromator, E—beam window 2, F—capillary optics, G—sample.

Table 2. Positions of simulated beamline components.

	Component	Distance from the Source [mm]
1	Fixed mask 1	2314
2	White beam slits	5122.5
3	Fixed mask 2	6704
4	White beam filters	8790
5	Be window 1 (250 μm)	9110
6	Monochromator	11,570
7	Be window 2 (500 μm)	12,625
8	Capillary optics	~14,450 (depending on the optic in use)
9	Sample	14,500

A DCM uses two crystals made of Si(111) that are precisely aligned to diffract X-rays of a specific wavelength with a bandwidth of $\sim 1.4 \times 10^{-4}$ and a constant vertical offset of 10 mm. The dimensions (width \times length) of the first and the second crystal are 35 mm \times 55.5 mm and 35 mm \times 140 mm, respectively. A DMM uses a pair of multilayer mirrors to diffract and reflect X-rays to achieve monochromatization with a bandwidth of several percent. Each mirror has two different stripes of multilayer structures next to each other. The first stripe was prepared to work with the energy range of 4–8 keV. It has a Ni/B₄C multilayer coating with 75 periods, a period of 4 nm and a metal layer thickness-to-period ratio of 0.4. The second stripe is dedicated to work in the 7.5–15 keV energy range. It has a Mo/B₄C multilayer coating with 115 periods, a period of 2.6 nm and a metal layer thickness-to-period ratio of 0.4. The dimensions of both stripes were set to 20 mm \times 280 for the stripes on the first optics, and to 20 \times 172 mm for the stripes on the second optics. The vertical offset between the second and the first crystal is again set to the fixed value of 10 mm.

In order to achieve the focused beam on the sample, two types of capillary optics will be used at PolyX. Seven different polycapillary lenses (from Helmut-Fisher formerly IfG, Germany and XOS, USA) will be interchangeably used to achieve a focal spot in range from 10 to 100 μm . A narrower beam will be achieved with an achromatic ellipsoidal single-bounce monicapillary lens (AEXML) with a 30 nm Pt coating from Sigray, USA. The details of the selected optical elements are given in Table 3 (the remaining polycapillaries are described in the supplementary materials).

Table 3. Parameters of simulated optics.

Alias	Working Distance [mm]	Optics Length [mm]	Optics Upstream Diameter [mm]	Optics Downstream Diameter [mm]	Upstream Capillary Channel Diameter [μm]	No. of Capillaries
poly f = 2.5	2.5	37	4.2	0.83	0.75	313,136
poly f = 14.5	14.5	63.75	6.4	2	3.3	97,801
poly f = 40	40	41	6.5	4.5	7.5	101,144
AEXML	20.5	50	1	0.54	-	1

The main measurement modes that will be routinely used at PolyX are elemental microimaging by μ -XRF, elemental speciation by μ -XAS and absorption/phase-contrast imaging by μ -CT. Other techniques that are planned to be available at the beamline are confocal-XRF for 3D elemental imaging, high-resolution plenoptic X-ray imaging and μ -XRD for crystalline phase speciation. Several different X-ray detectors will be installed at the end station. The first group—spectrometry detectors—is composed of two silicon drift detectors (SDD) with 80 mm² active area (one with 25 μm Be window and one with ML3.3 Extreme window) by Hitachi High-Tech. As a digital pulse processor, a DANTE

system from XGLab will be used. The detectors will work in the back-scatter geometry (at 45° with the sample perpendicular to the beam); however, the standard $45^\circ/45^\circ$ geometry will be also achievable. The ultra-thin ML3.3 window was chosen to allow the detection of low-energy X-rays in a helium atmosphere. The second class of detectors are those devoted to imaging: hybrid pixel EIGER 2S 1 M with $77.1 \times 79.7 \text{ mm}^2$ active area ($75 \times 75 \mu\text{m}^2$ pixel size) by Dectris and white beam microscope by OptiquePeter with variable scintillators and Edge 5.5 sCMOS camera (2560×2160 pixel) by PCO. The third class of detectors will be beam monitors: ionisation chambers by FMB Oxford and PIN Diodes by Hamamatsu. The key design aspect of the experimental station is to allow multi modal experiments as well as easy switching between different modes.

3. Methods

In this work, we used a Python-based library XRT [5] to perform ray-tracing simulations of the standard beamline components. The simulations covered all crucial components of the beamline, including the bending magnet source characterised by parameters from Table 1. Other elements simulated by XRT are slits and masks, beryllium windows, filters, a double crystal monochromator (DCM) or a double multilayer monochromator (DMM), as well as an ellipsoidal single-bounce monochromator (AEXML). Additionally, the polycap library [7] combined with XRT library was used to perform efficient ray tracing of the beamline with the polycapillary lenses.

The simulation took into account the expected distances from the source for every element, as listed in Table 2. For all simulations of DCM, the beam was slit down vertically to keep the bandwidth $dE/E = 0.02\%$.

The combination of XRT and polycap libraries enabled an efficient modeling of the whole beamline. The XRT was used to obtain the rays at the entrance surface of polycapillary, and polycap ray-traced X-ray propagation inside polycapillary device. Importantly, the parameters (position, direction, polarization) of each ray were directly transferred from xrt to polycap by in-house developed write/read Python functions.

The simulations of polycapillary optics were performed with the assumption that all of them had ellipsoidal shapes. The parameters of simulated lenses are presented in Table 2. The naming of polycapillary lenses (aliases) was based on their working distances. For AEXML optics, the distortion from perfect shape was implemented as a slope error of $10 \mu\text{rad}$ (RMS), in order to estimate a realistic spot size. In Figures 2–4, the examples of ray visualizations are presented, just upstream of the entrance to polycapillary and monochromator lenses as well as in their focal planes. The left panels of Figures 2 and 3 (created with the XRT library visualisation tool) show spatial distributions of the simulated rays together with their projections on vertical and horizontal axes. The right panels show energy distributions. The position and energy mean values with FWHM values are also given. N_{all} and N_{good} are values of all simulated rays and rays reflected within the working optical surfaces, respectively. The total photon flux (Φ) is also given.

The simulations of X-ray spectra were carried out with the XMI-MSIM tool. The number of photons per interval and discrete line were set to 10,000 and 100,000, respectively. The single interaction per photon trajectory was simulated, and Poisson noise was generated. The default detector response was used.

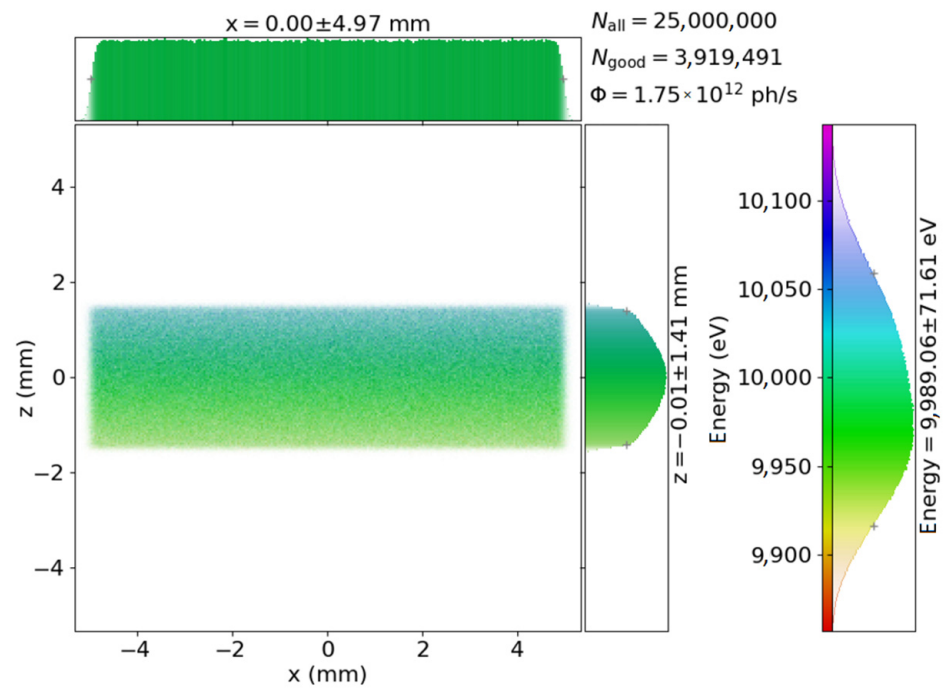


Figure 2. Visualizations of simulated beam upstream the entrance of lenses. The mean beam energy of 10 keV was achieved with DMM. White beam slits closed to $3.53 \text{ mm} \times 1.06 \text{ mm}$.

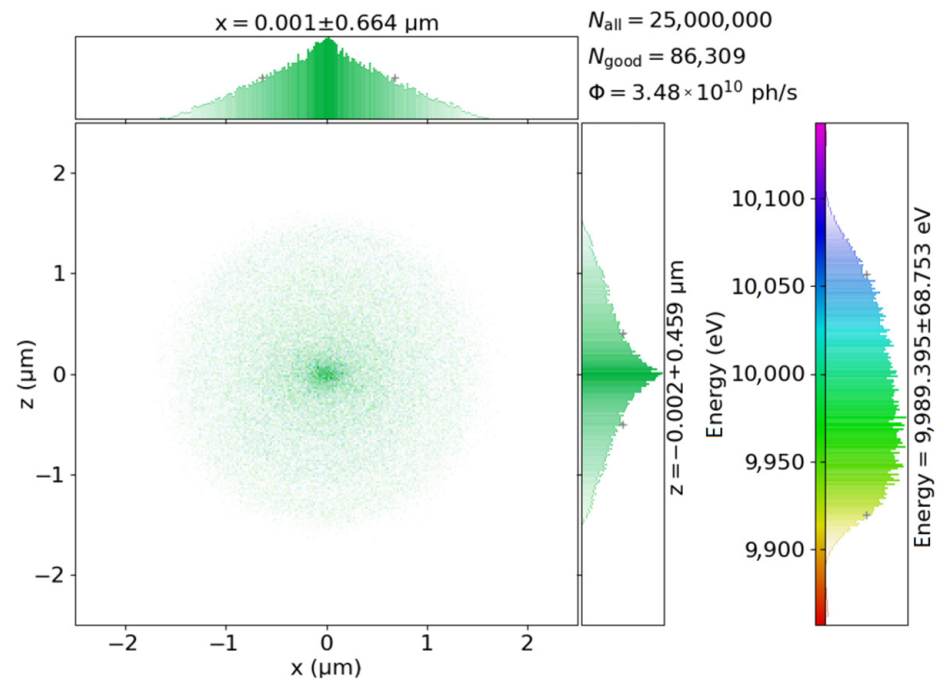


Figure 3. Visualizations of simulated rays at focal plane of monocapillary lens. The mean beam energy of 10 keV was achieved with DMM. White beam slits closed to $3.53 \text{ mm} \times 1.06 \text{ mm}$.

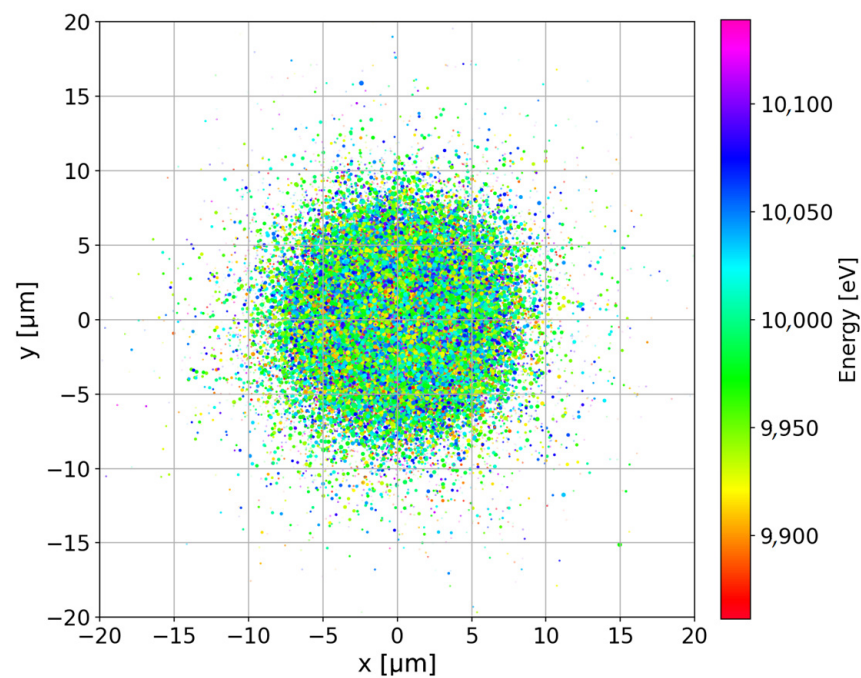


Figure 4. Visualizations of simulated rays at focal plane of polycapillary lens. The mean beam energy of 10 keV was achieved with DMM. White beam slits closed to 3.53 mm \times 1.06 mm.

4. Results and Discussion

Our simulations were performed using a range of configurations for the beamline components and X-ray focusing optics. The results of the simulations were used to evaluate the X-ray beam properties, including the flux, the spot size, and energy resolution for different configurations.

First, we performed simulations of the beamline for the white beam mode, i.e., without any monochromator. To shape the X-ray spectrum, Al filters of variable thickness (0.01 mm, 0.05 mm, 0.1 mm, 0.25 mm, 0.5 mm, 1 mm) were simulated. White beam energy spectra and the total flux (denoted as N in the legend) were simulated for full vertical beam size and for 1 mrad horizontal slit opening (Figure 5).

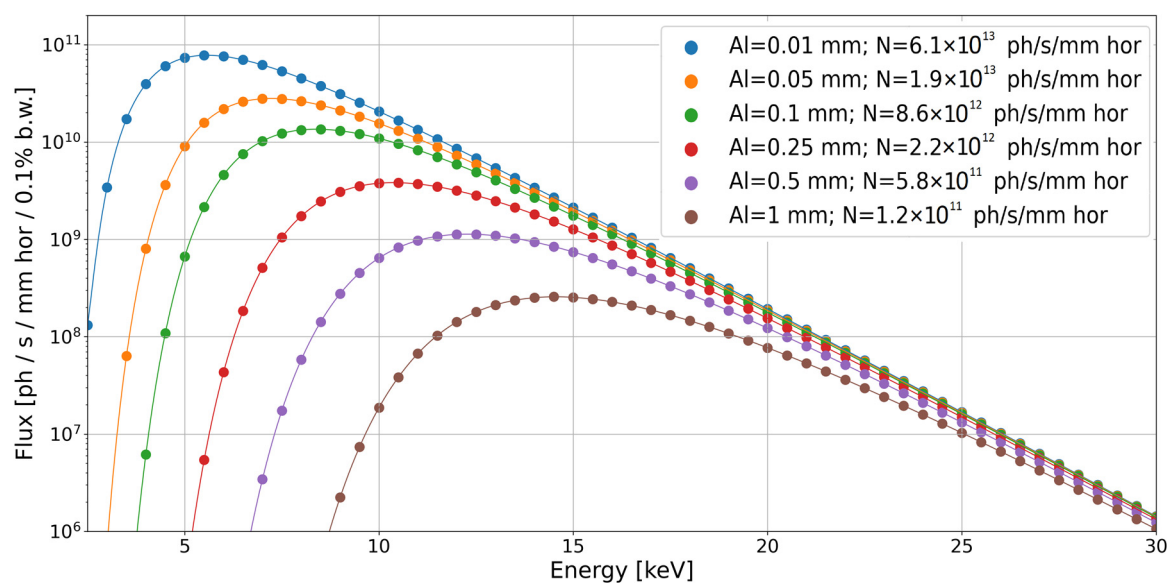


Figure 5. Simulated flux for unfocused white beam and Al filters with different thicknesses. In the figure legend, N denotes the energy-integrated flux.

Next, we calculated the flux for both monochromator types, DCM and DMM. For DMM, both stripes were simulated for the relevant energy ranges. The results are shown in Figure 6.

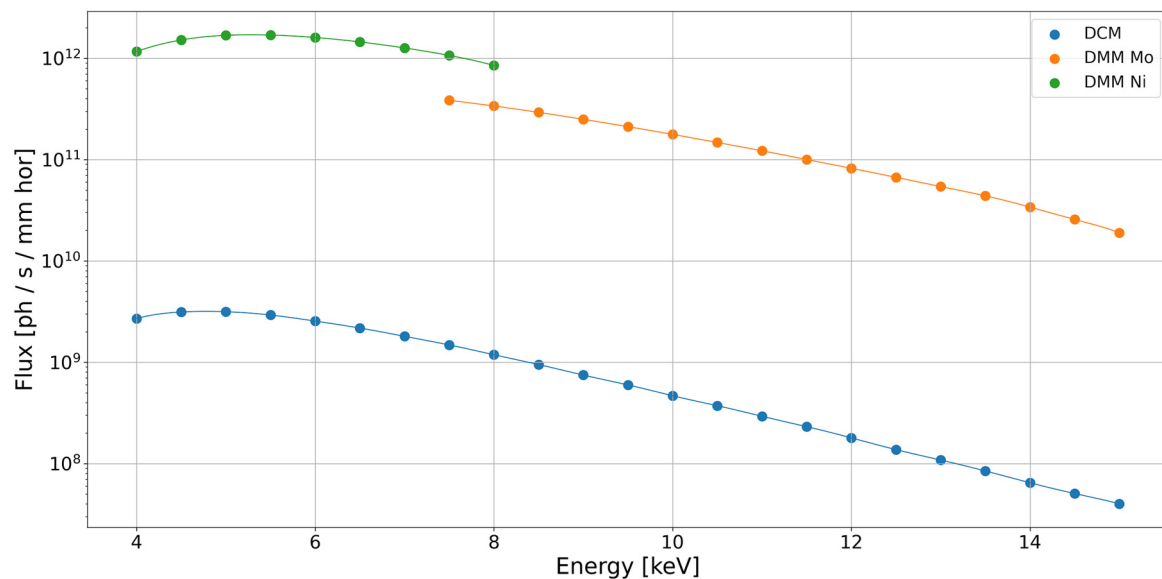


Figure 6. Simulated flux for unfocused beam after DCM and DMM monochromators. For DCM, the beam was slit down vertically to keep a bandwidth of $dE/E = 0.02\%$.

Subsequently, we focused on the prediction of achievable beam parameters, while using different capillary optics. For the sake of clarity, the next figures show results for only three types of polycapillary lenses and for one monocapillary lens. However, the supplementary materials present selected results for the other four available polycapillary lenses.

The transmission efficiencies of the focusing elements (Figure 7) were calculated by performing the following steps: (i) slits were set to be fully opened in the vertical and horizontal directions, (ii) a simulation for the white beam was conducted (without any Al filters) for different energies, in the range of 4–15 keV, the step between the points was 0.5 keV, and bandwidth for every step was 0.1%, (iii) the flux N_0 was calculated for rays that were accepted into the optics entrance, (iv) the flux N was calculated in the focal spots, and (v) the transmission was calculated as $T = N/N_0$.

The transmission efficiency for AEXML is significantly higher than for polycapillary optics since, in contrast to polycapillary optics, it relies on single-bounce transmission. AEXML optic has two distinguishable drops, which are caused by the L absorption edges of the platinum inner coating.

The spot sizes in the focal planes (Figures 8 and 9) were estimated using the same white beam simulations as described above for transmission efficiencies. First, vertical and horizontal histograms of the rays were calculated, then histograms of FWHMs were determined for both axes and the average value was taken as the final spot size.

For polycapillary lenses and for an ellipsoidal single-bounce monocapillary lens, the full energy spectra for the beams that passed through the optics were estimated during the simulations. These results were used to calculate the achievable fluxes in the focal spot. For the white beam mode, the different thicknesses of Al filters were used in simulations (Figure 10). The flux was also estimated for the beam that passed through one of the monochromators (DCM or DMM described in the previous section) and later focused by the lenses (Figure 11). The results for a subset of simulated lenses are presented in supplementary materials.

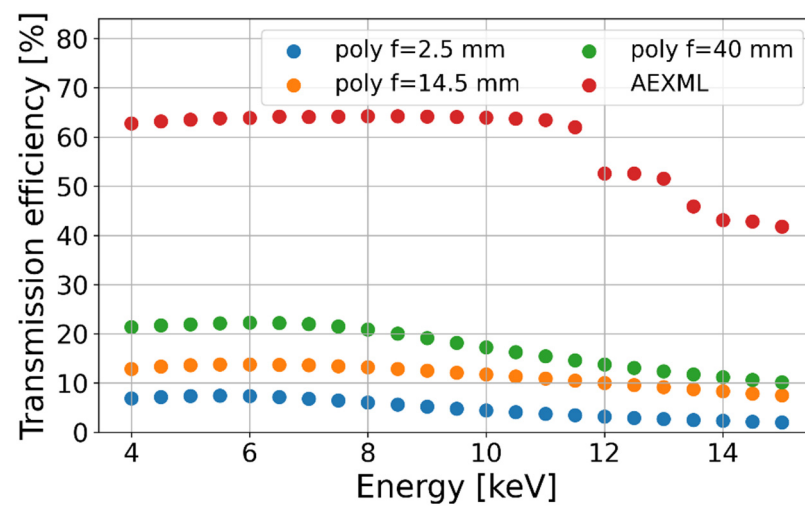


Figure 7. Simulated transmission efficiencies for polycapillary lenses and an ellipsoidal monicapillary lens. All steps were performed by simulating white beam with fully opened slits in vertical and horizontal directions.

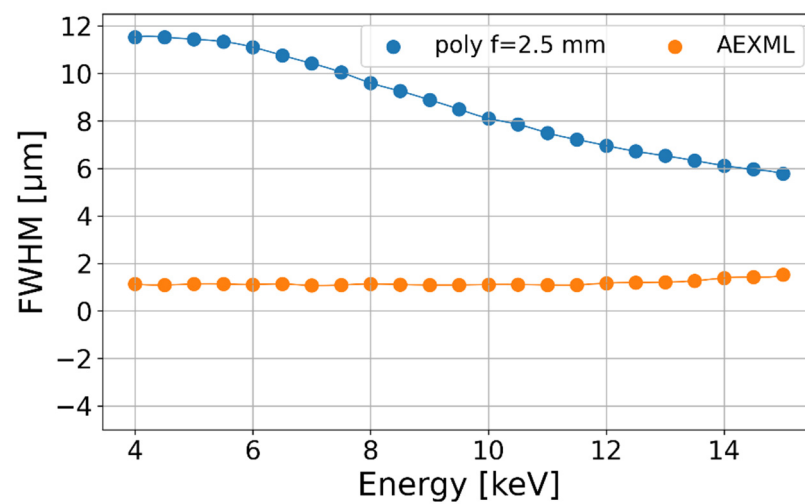


Figure 8. Simulated spot sizes for polycapillary lens and an ellipsoidal monicapillary lens.

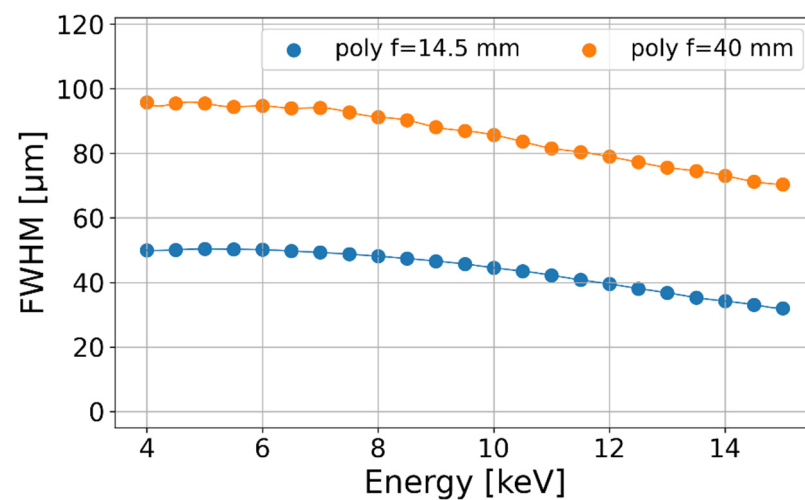


Figure 9. Simulated spot sizes for polycapillary lenses.

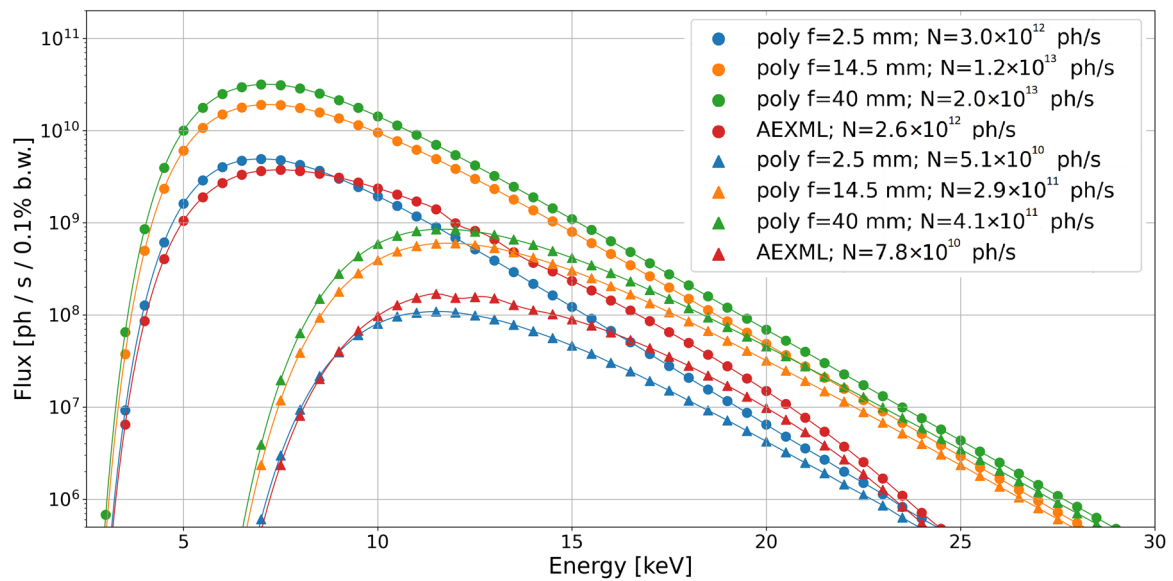


Figure 10. Simulated flux for X-ray beam focused with polycapillary lenses and an ellipsoidal monicapillary lens in white beam mode and Al filters with different thicknesses (dot markers—0.05mm, triangle markers—0.5mm). N denotes the total, i.e., energy-integrated flux.

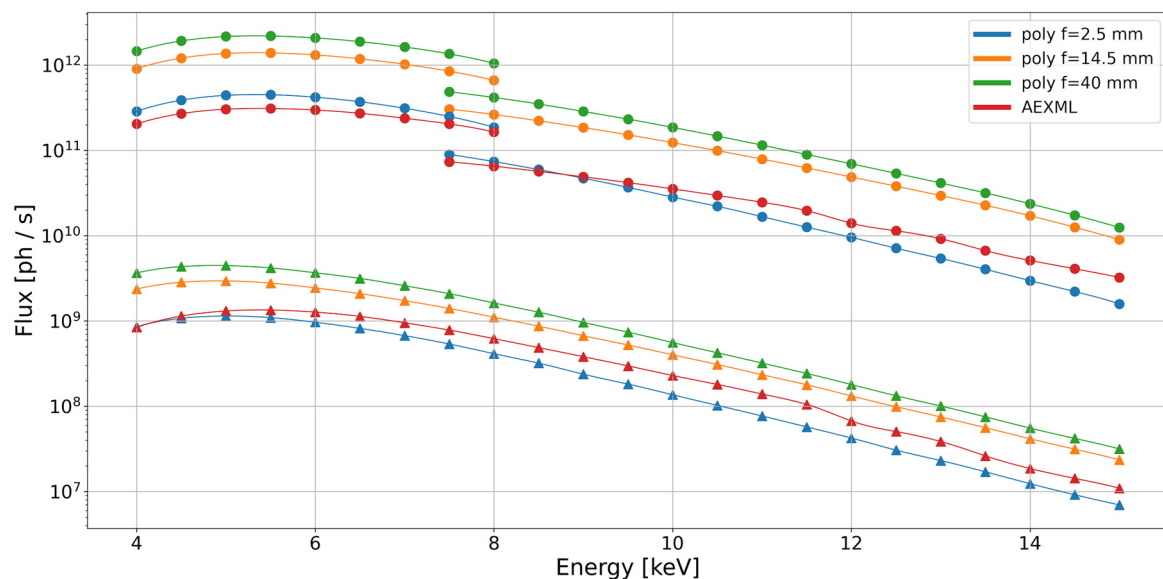


Figure 11. Simulated flux for X-ray beam focused with polycapillary lenses and an ellipsoidal monicapillary lens. Triangles—DCM, Dots—DMM. For DCM, beam was slit down vertically to keep the bandwidth $dE/E = 0.02\%$.

To predict the results of μ -XRF experiments, simulations of the X-ray fluorescence spectra from two different samples were performed with XMI-MSIM. Simulations were performed for the beam focused with AEXML, as a worst-case scenario in terms of expected beam intensity and the best scenario in terms of spatial resolution. All the simulations were carried out for a silicon drift detector equipped with ML3.3 Extreme window, helium atmosphere and backscatter geometry (90° angle between the beam and the sample plane and 45° angle between the sample plane and the detector axis) with a sample-detector distance of 3 cm and an acquisition time of 1 s. Two excitation modes were chosen: monochromatic (5 keV, 10 keV and 15 keV) with DMM and polychromatic with the white beam filtered with various aluminium filters. The sample of biological thin tissue section ($4 \mu\text{m}$), one of the most demanding materials, was chosen. The elemental composition of

the tissue was selected based on the literature data [15] and is given in Table 4, together with the simulated elemental intensities. The simulated spectra for both excitation modes are shown in Figures 12 and 13. As can be seen for 5 keV, 10 keV, and white beam filtered with 1 mm Al, the expected count rates of the elements up to zinc are high enough to make fast XRF imaging feasible even with the acquisition times being much lower than 1 s. Heavier and low-abundant elements like Se, Br, Rb and Sr can be efficiently excited with only the polychromatic beam; however, the detection of those elements will be very difficult due to the poor signal-to-noise ratio.

Table 4. Elemental composition and intensities of K α lines (in counts per second) for simulated thin tissue sample.

Z	Elem.	Weight Fraction		DMM			White Beam Filtered with Al		
		Value	Unit	5 keV	10 keV	15 keV	0.5 mm	1 mm	2 mm
1	H	8.1	%						
6	C	64.8	%						
7	N	9.8	%						
8	O	13.7	%						
11	Na	0.2	%	1600	23	<1	380	47	4
12	Mg	620	$\mu\text{g/g}$	530	17	<1	290	35	3
15	P	1.2	%	110k	1800	45	30k	3800	310
16	S	0.8	%	110k	1800	46	30k	3800	320
17	Cl	0.3	%	58k	1000	26	16k	2100	180
19	K	1.0	%	380k	6900	180	120k	15k	1300
20	Ca	130	$\mu\text{g/g}$	6800	120	3	2100	270	22
25	Mn	10	$\mu\text{g/g}$	-	29	<1	510	66	6
26	Fe	210	$\mu\text{g/g}$	-	770	21	13k	1700	150
29	Cu	120	$\mu\text{g/g}$	-	710	21	11k	1600	150
30	Zn	180	$\mu\text{g/g}$	-	1200	36	18k	2800	250
34	Se	2	$\mu\text{g/g}$	-	-	<1ss	110	32	4
35	Br	3	$\mu\text{g/g}$	-	-	<1	120	65	6
37	Rb	35	$\mu\text{g/g}$	-	-	-	700	310	67
38	Sr	95	$\mu\text{g/g}$	-	-	-	1200	600	160

In order to acquire information about the capabilities of analysis of higher Z elements with the high-energy tail of the polychromatic excitation spectrum, a 1mm-thick soda-lime glass (72% SiO₂, 14% Na₂O, 12% CaO, 2% Al₂O₃) sample doped with some elements (Se, Sr, Zr, Mo, W, Pb, Th, U) at 100 $\mu\text{g/g}$ level was used. The results of the simulations for 1 mm, 2 mm and 4 mm aluminium filters are shown in Table 5 and Figure 14. Since the high energy limit of the DMM monochromator is at 15 keV, high Z elements cannot be excited with the monochromatic beam (Sr, Zr on K shell and Th, U on L shell). However, Figure 14 indicates that they can still be efficiently excited by the hardened white beam allowing analysis of such elements in samples of, i.e., geological origin.

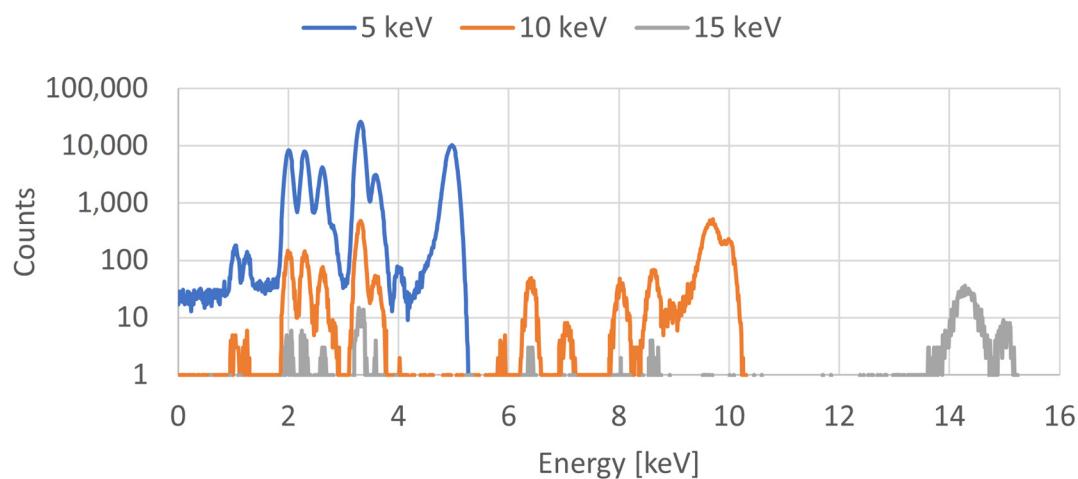


Figure 12. Simulated XRF spectra of thin tissue slice sample excited with monochromatic beam focused by AEXML.

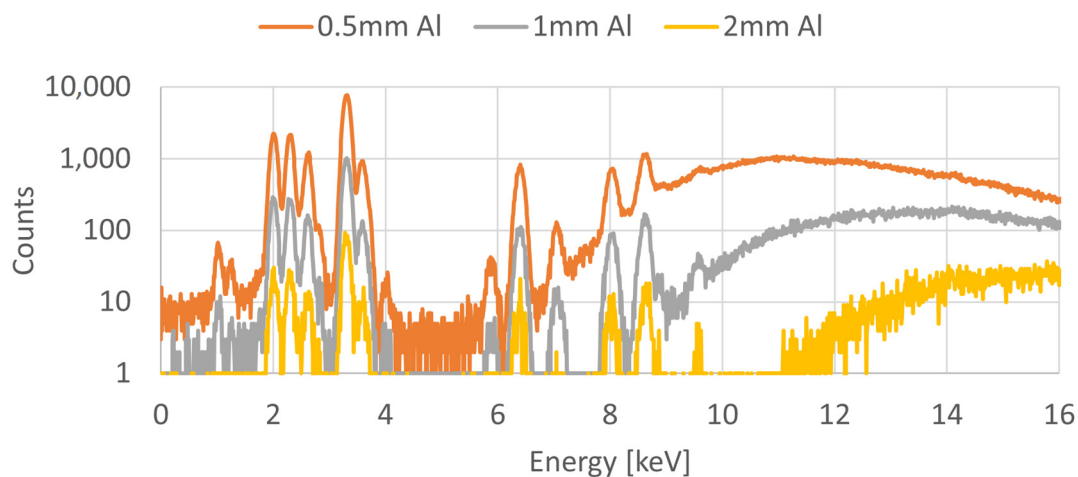


Figure 13. Simulated XRF spectra of thin tissue sample excited with polychromatic beam focused by AEXML.

Table 5. Elemental XRF intensities (in counts per second) for simulated glass sample.

	Elem.	Line	Weight Fraction [$\mu\text{g/g}$]	1 mm Al	2 mm Al	4 mm Al
34	Se	K α	100	120k	17k	990
38	Sr	K α		92k	24k	2300
40	Zr	K α		50k	17k	2500
42	Mo	K α		19k	8400	1700
74	W	L α		24k	2400	130
82	Pb	L α		44k	6800	440
90	Th	L α		30k	8000	840
92	U	L α		23k	7300	890

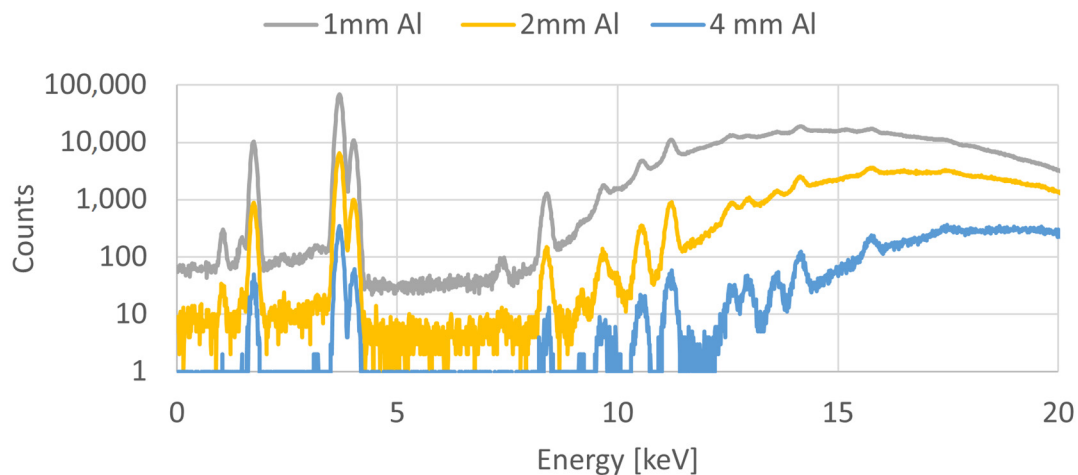


Figure 14. Simulated spectra of glass sample excited with polychromatic beam focused by AEXML.

5. Conclusions

In this work, we demonstrated the physical model of the PolyX beamline created by combining two ray-tracing tools: XRT [5] and polycap libraries [7], which allowed us to simulate all crucial components of the beamline, including the polycapillary optics. The estimated flux was presented for different beamline configurations: (i) unfocused and focused white beam with various Al filters, (ii) DCM monochromator for unfocused and focused beam, and (iii) two types of DMM monochromators for unfocused and focused beam. Additionally, properties like transmission efficiencies and spot sizes were calculated for capillary lenses and AEXML. The results give better insight into the expected performance of the PolyX beamline and will be confronted with experimental data in the near future. The applied ray-tracing model can be also used for the preparation of different experiments in multiple measurement modes accessible at the end station. For example, an extension of the presented approach to simulate multi-beam X-ray imaging [16] or von Hamos spectrometers [17] seems to be feasible. The simulations of the X-ray spectra recorded for thin tissue slice samples with AEXML are very promising in terms of high-resolution, fast μ -XRF imaging of elements up to zinc.

Supplementary Materials: The following supporting information can be downloaded at: <https://www.mdpi.com/article/10.3390/app14177486/s1>. Data for four additional polycapillary lenses are presented in Supplementary Materials. It includes parameters of the lenses (Table S1), transmission efficiency (Figure S1), spot sizes (Figure S2), flux distribution in white beam mode (Figure S3), and flux with DMM and DCM (Figure S4).

Author Contributions: Conceptualisation: P.K.; Methodology: F.K., P.W. and T.K.; Software: F.K.; Validation: F.K. and T.K.; Investigation: F.K. and P.W.; Writing—original draft: F.K.; Writing—review and editing: P.W., T.K., K.M.S. and P.K.; Visualisation: F.K. and P.W.; Supervision: P.W., M.S.-B. and P.K.; Project administration: K.M.S. and P.K.; Funding acquisition: P.K. All authors have read and agreed to the published version of the manuscript.

Funding: This publication was partially developed under the provision of the Polish Ministry of Science and Higher Education project “Support for research and development with the use of research infrastructure of the National Synchrotron Radiation Centre SOLARIS” under contract no 1/SOL/2021/2.

Institutional Review Board Statement: Not applicable.

Informed Consent Statement: Not applicable.

Data Availability Statement: Data presented in this study are available on request from the corresponding author.

Acknowledgments: We are very grateful to Błażej Ruszczycki for his help in proofreading the manuscript.

Conflicts of Interest: The authors declare no conflicts of interest.

References

1. Szlachetko, J.; Szade, J.; Beyer, E.; Blachucki, W.; Ciochoń, P.; Dumas, P.; Freindl, K.; Gazdowicz, G.; Glatt, S.; Guła, K.; et al. SOLARIS National Synchrotron Radiation Centre in Krakow, Poland. *Eur. Phys. J. Plus* **2023**, *138*, 10. [\[CrossRef\]](#)
2. Sowa, K.M.; Wróbel, P.; Kołodziej, T.; Blachucki, W.; Kosiorowski, F.; Zajac, M.; Korecki, P. PolyX beamline at SOLARIS—Concept and first white beam commissioning results. *Nucl. Instrum. Methods Phys. Res. Sect. B* **2023**, *538*, 131–137. [\[CrossRef\]](#)
3. Sowa, K.M.; Kujda, M.P.; Korecki, P. Plenoptic x-ray microscopy. *Appl. Phys. Lett.* **2020**, *116*, 014103. [\[CrossRef\]](#)
4. del Rio, M.S.; Canestrari, N.; Jiang, F.; Cerrina, F. SHADOW3: A new version of the synchrotron X-ray optics modelling package. *J. Synchrotron Radiat.* **2011**, *18*, 708–716. [\[CrossRef\]](#) [\[PubMed\]](#)
5. Klementiev, K.; Chernikov, R. Powerful scriptable ray tracing package xrt. In *Advances in Computational Methods for X-ray Optics III, Proceedings of the SPIE Optical Engineering + Applications, San Diego, CA, USA, 17–21 August 2024*; SPIE: Bellingham, WA, USA, 2024; Volume 9209. [\[CrossRef\]](#)
6. Bergbäck Knudsen, E.; Prodi, A.; Baltser, J.; Thomsen, M.; Kjær Willendrup, P.; Sanchez del Rio, M.; Ferrero, C.; Farhi, E.; Haldrup, K.; Vickery, A.; et al. McXtrace: A Monte Carlo software package for simulating X-ray optics, beamlines and experiments. *J. Appl. Crystallogr.* **2013**, *46*, 679–696. [\[CrossRef\]](#)
7. Tack, P.; Schoonjans, T.; Bauters, S.; Vincze, L. An X-ray ray tracing simulation code for mono- and polycapillaries: Description, advances and application. *Spectrochim. Acta—Part B At. Spectrosc.* **2020**, *173*, 105974. [\[CrossRef\]](#)
8. Vincze, L.; Janssens, K.; Adams, F.; Rindby, A. Detailed ray-tracing code for capillary optics. *X-ray Spectrom.* **1995**, *24*, 27–37. [\[CrossRef\]](#)
9. Yang, J.; Li, Y.D.; Wang, X.Y.; Zhang, X.Y.; Lin, X.Y. Simulation and application of micro X-ray fluorescence based on an ellipsoidal capillary. *Nucl. Instrum. Methods Phys. Res. Sect. B* **2017**, *401*, 25–28. [\[CrossRef\]](#)
10. Lin, X.-Y.; Li, Y.-D.; Sun, T.-X.; Pan, Q.-L. Simulation of x-ray transmission through an ellipsoidal capillary. *Chin. Phys. B* **2010**, *19*, 070205. [\[CrossRef\]](#)
11. Vincze, L.; Kukhlevsky, S.V.; Janssens, K. Simulation of polycapillary lenses for coherent and partially coherent X-rays. In *Advances in Computational Methods for X-ray and Neutron Optics, Proceedings of the Optical Science and Technology, the SPIE 49th Annual Meeting, Denver, CO, USA, 2–6 August 2004*; SPIE: Bellingham, WA, USA, 2004; Volume 5536. [\[CrossRef\]](#)
12. Peng, S.; Liu, Z.; Sun, T.; Wang, K.; Yi, L.; Yang, K.; Chen, M.; Wang, J. Simulation of transmitted X-rays in a polycapillary X-ray lens. *Nucl. Instrum. Methods Phys. Res. Sect. A* **2015**, *795*, 186–191. [\[CrossRef\]](#)
13. Hampai, D.; Dabagov, S.B.; Cappuccio, G.; Cibir, G. X-ray propagation through polycapillary optics studied through a ray tracing approach. *Spectrochim. Acta B* **2007**, *62*, 608–614. [\[CrossRef\]](#)
14. Schoonjans, T.; Vincze, L.; Solé, V.A.; del Rio, M.S.; Brondeel, P.; Silversmit, G.; Appel, K.; Ferrero, C. A general Monte Carlo simulation of energy dispersive X-ray fluorescence spectrometers—Part 5: Polarized radiation, stratified samples, cascade effects, M-lines. *Spectrochim. Acta Part B* **2012**, *70*, 10–23. [\[CrossRef\]](#)
15. Szczerbowska-Boruchowska, M. Sample thickness considerations for quantitative X-ray fluorescence analysis of the soft and skeletal tissues of the human body—Theoretical evaluation and experimental validation. *X-ray Spectrom.* **2012**, *41*, 328–337. [\[CrossRef\]](#)
16. Sowa, K.M.; Jany, B.R.; Korecki, P. Multipoint-projection x-ray microscopy. *Optica* **2018**, *5*, 577. [\[CrossRef\]](#)
17. Blachucki, W.; Sowa, K.M.; Kołodziej, T.; Wróbel, P.; Korecki, P.; Szlachetko, J. First white beam on a von Hámos spectrometer at the PolyX beamline of SOLARIS. *Nucl. Instrum. Methods Phys. Res. Sect. B* **2023**, *542*, 133–136. [\[CrossRef\]](#)

Disclaimer/Publisher’s Note: The statements, opinions and data contained in all publications are solely those of the individual author(s) and contributor(s) and not of MDPI and/or the editor(s). MDPI and/or the editor(s) disclaim responsibility for any injury to people or property resulting from any ideas, methods, instructions or products referred to in the content.